A Novel Approach for Fault Location of Overhead Transmission Line With Noncontact Magnetic-Field Measurement

Qi Huang, *Senior Member, IEEE*, Wei Zhen, and Philip W. T. Pong

***Abstract*—Prompt and accurate location of faults in a large-scale transmission system can accelerate system restoration, reduce outage time, and improve system reliability. Traditional approaches are categorized into traveling-wave-based and impedance-based measurement techniques. The traveling-wave-based approach requires detection devices to connect to the high-voltage transmission line, making the solution complex and costly. And the impedance-measurement-based approach is highly dependent on the quality of the signal and affected by fault resistance, ground resistance and non-homogeneity in line configuration. Hence, these approaches may cause a location error that is unacceptable in certain operation cases. In this paper, a novel approach based on noncontact magnetic-field measurement is proposed. With the magnetic field measured along the transmission line by using highly sensitive, broadband, and a low-cost magnetoresistive magnetic sensor, the fault span can be located. The collected data can be further used for identifying the fault type and location within the fault span. The overall system was designed and numerical simulations were performed on typical tower configurations. The simulated results verify the validity of the proposed scheme.**

***Index Terms*—Fault location, magnetoresistive magnetic sensor, noncontact magnetic-field measurement, overhead transmission line.**

I. Introduction

OVERHEAD transmission lines are most commonly used for delivering electric power from source locations to distribution networks. The rapid growth of electric power systems over the past few decades has resulted in a large increase of the number of lines in operation and their total length. These lines are exposed to faults as a result of lightning, short circuits, faulty equipment, misoperation, human errors, overload, growing vegetation (or swaying trees), aging, etc. [1]–[3]. Statistics show that line faults are the most common fault in power systems [4]. When a fault occurs on an electrical transmission line, it is very important to detect it and to find its location in order to take necessary remedial actions and to restore power as soon as possible. The time needed to determine the fault point along the line affects the quality of the power delivery and, hence, the overall efficiency of the power networks. These concepts are gaining increasing importance these days because the new policies for deregulation and liberalization of power and energy markets may lead to more stressed operation and decreased reliability levels in transmission systems due to the pursuit of profit [5].

Engineers and researchers have been trying to find a reliable and efficient way for estimating fault location. The currently available fault detection and location methods can be broadly classified into two types [6]: 1) traveling-wave technique and 2) impedance-measurement-based technique. In the traveling-wave technique, either the transient created by a fault is captured or impulses are injected into the line, and the reflected traveling wave is detected with time-domain reflectometery (TDR). The fault location is then determined by timing analysis of the traveling wave. As the faulted signal obtained at the end of the transmission line is highly mingled with noise, some modern signal processing techniques, such as the wavelet [7], are used for fault location. In the impedance-measurement-based technique, the voltage and current during prefault and postfault are acquired and analyzed. The line parameters can then be calculated with the transmission-line model and the fault can be located. These methods may be one ended, two ended, or even multiended, depending on how the receiving devices are deployed. Since the development of relay protection is advancing fast, it is now possible to collect the data from the synchronized phasor measurement unit embedded in a digital relay or a fault recorder in order to achieve the goal of fault location [8]. It is proved that the synchronized measurement would improve the performance of fault location.

All of the aforementioned methods produce reasonable fault-location results. However, all of these methods need to connect a device to the high-voltage transmission line and the required devices are generally costly. For example, in the traveling-wave-based approach, the accuracy of the location is highly dependent on the performance of the costly high-speed data-acquisition system. Furthermore, these methods fully depend on an assumption that the parameters of the transmission line are uniform.

Manuscript received April 12, 2011; revised October 07, 2011, November 27, 2011, December 22, 2011, and February 15, 2012; accepted March 05, 2012. Date of publication April 17, 2012; date of current version June 20, 2012. This work was supported in part by the Natural Science Foundation of China under Grant 50977007) and in part by the Program for New Century Excellent Talents in University under Grant NCET-09-0262). Paper no. TPWRD-00287-2011.

Q. Huang is with the Sichuan Provincial Key Lab of Power System Wide-Area Measurement and Control, University of Electronic Science and Technology of China (UESTC), Chengdu 611731, Sichuan, China (e-mail: hwong@uestc.edu.cn).

W. Zhen is with the Sichuan Provincial Key Lab of Power System Wide-Area Measurement and Control. He is also with Sichuan Electric Power Test and Research Institute, Chengdu 610072, Sichuan, China (e-mail: zhenwei34156@163.com).

P. W. T. Pong is with the Department of Electrical and Electronic Engineering, the University of Hong Kong, Hong Kong, China (e-mail: ppong@eee.hku.hk).

Color versions of one or more of the figures in this paper are available online at http://ieeexplore.ieee.org.

Digital Object Identifier 10.1109/TPWRD.2012.2190427

Considering the fact that the transmission lines are distributed over a large geographical area, this assumption is generally not entirely true. For example, the nonuniform spacing of the phase conductors may affect the inductance (although phase conductors are transposed to reduce the effect), temperature may affect the resistance, and sag may affect the capacitance in different transmission-line segments [10]. Operation experience shows that most of the systems can limit the fault-location error within 1–2% of the monitored line length. In certain cases, the error may reach 5% or even more [11]. The accuracy factor becomes even more important for long transmission lines because even a relatively small error would result in an uncertainty of a few kilometers, causing significant delay for the maintenance crew to find the fault location [11]. Especially in areas over rough terrain (e.g., mountain area, such as Liangshan of China), the installed system may cause an error of ± 3 km in 500-kV transmission lines. The maintenance crew may have to walk 6 km in a mountainous area to determine the exact location of the fault point. For nonpermanent faults, such as flashover caused by sag of stressed lines, considering their temporary nature, it may take even more effort to locate the fault point with these systems because the fault is not permanent and the system may have already resumed its normal condition by the time the maintenance crew arrives.

This paper introduces a low-cost high-precision solution, which does not need to connect the device to the HV transmission line and is highly sensitive for fault location. The new method proposed here uses a novel type of sensitive magnetoresistive (MR) magnetic sensor to measure the transient current. The sensors are placed on the tower, and the data are transmitted to a data-processing center where analysis software can determine which span the fault location belongs to. The collected magnetic-field data can also be used to identify the fault type and even locate within the fault span.

The rest of this paper is organized as follows. Section II introduces this novel technique of using the MR magnetic sensor for fault-location purposes. The design of the location system is described in Section III. Numerical simulations were performed to verify the proposed scheme and are presented in Section IV. Section V identifies the effectiveness of the proposed approach by performing error estimation and comparison of available methods. Section VI concludes this paper.

II. Fault Detection With a Novel Type of Magnetic-Field Sensor

Most of the faults in power systems are short circuit related [12]. Hence, the fault detection may be accomplished by the comparison of the current under normal conditions and fault conditions, and the current measurement can be achieved by the magnetic-field measurement.

Traditional current measurement, by using Ampere's law, involves placing a coil to wind around the conductor. In HV engineering applications, this is not an ideal solution since one needs to put the coil close to the HV conductors. Current measurement can actually be carried out by the magnetic-field measurement. Once there is current flowing in a conductor, there will be a magnetic field generated around the conductor. The magnetic-field strength increases with its line ampacity. The strength, direction, and distribution of the magnetic field emanated from the conductors contain information about the electric power parameters, such as amplitude, frequency, and phase of the electric current. It is noticed that measurement based on the modern magnetic-field sensor can provide accurate and reliable data without physical contact.

Attributed to the fast advancement of the microelectromechanical systems (MEMS) packaging technology and magnetoresistance material technology, the MR magnetic sensors, based on the magnetoresistance effect, are widely used in many applications [13], [14]. Magnetoresistance is the property of a material to change the value of its electrical resistance when an external magnetic field is applied to it. Recently, the anisotropic magnetoresistance (AMR), giant magnetoresistance (GMR), and tunneling magnetoresistance (TMR) materials are discovered and integrated into commercial magnetic-field sensors successfully. These sensors, in general, have high sensitivity, large temperature range, and wide frequency bandwidth (from dc to several megahertz). The recent advances in MR sensors make it possible to fabricate low-cost chip-scale magnetometers for detecting the 3-D vector magnetic field [15].

The measurement of power systems with magnetic sensors has long been studied by many researchers [14], [16]–[18]. It would be ideal to deploy only a single sensor to measure the magnetic field generated by a single straight transmission line in a carefully shielded environment. Nevertheless, this approach will be impractical when applied to the power system current measurement; simply noted that the power system is a multiconductor entity, and the magnetic field produced around one transmission cable is overlaid by those of adjacent currents. Moreover, the strength of the earth's magnetic field and geomagnetic noise are not negligible since the sensor "views" them as dc and high-order harmonics, respectively. In order to improve the accuracy of the measuring system and reduce the crosstalk effects of other magnetic fields, multiple magnetic sensors are placed in the space around a conductor (or multiple conductors) to form a magnetic sensor array [18]. However, these measurements only deal with steady-state current. Since there is transient current present under fault conditions, MR sensors are very suitable for the measurement of fault current for their wide bandwidth. Besides the noncontact and wideband characteristics, the monitoring terminal can be made compact and low cost with these sensors. When the exact record of the transient current is to be recovered, a sensor array should be used and the signal-processing algorithm as well as placement of the sensor array should be properly designed.

III. Design of the Location System

A. Overall Scheme

For the fault-location application, it is already adequate if one can accurately locate the fault in a certain span (ranging from 400 to 1000 m). Once the place of the faulted span is known, it is relatively easy for the line inspector to locate the specific point of the fault within the span. In this scheme, we propose installing sensitive MR sensors at every tower. (For the long span, an additional monitoring terminal can be added in the middle

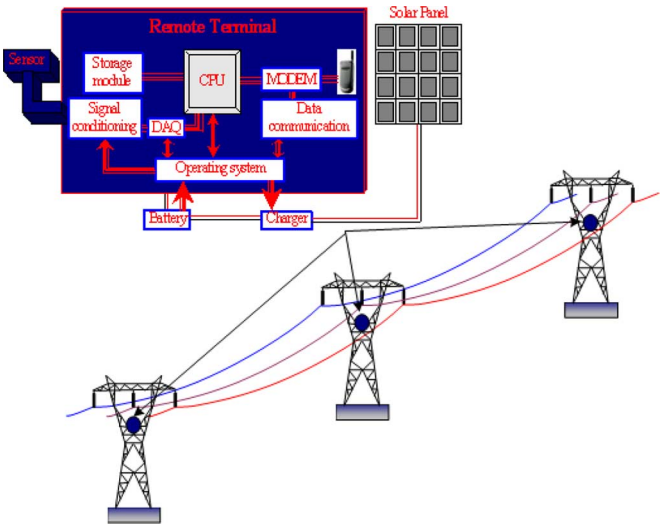

Fig. 1. Overall scheme of the proposed solution for fault location in HV transmission lines. (The circles indicate the positions of sensors.)

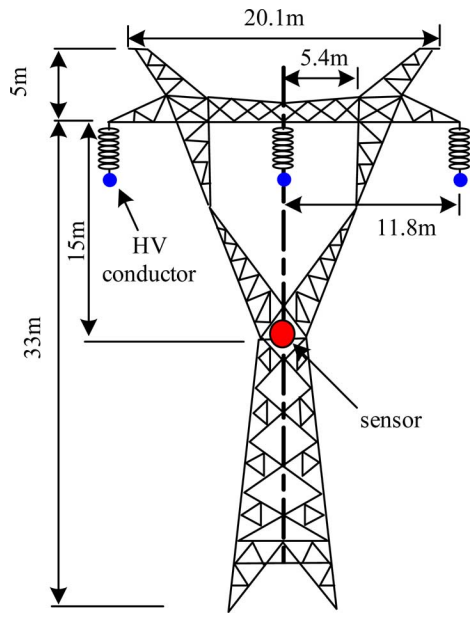

Fig. 2. Demonstration of installing the magnetic sensor on a typical 500-kV transmission tower.

since the devices of a terminal are cheap and they can work at a place far away from the current-carrying conductors.) The overall scheme of the proposed solution is shown in Fig. 1. The data collected from the remote monitoring terminals can be visualized in client software with the aid of the geographical information system (GIS) to help the operating crew locate the fault position promptly.

B. Remote Monitoring Terminal

The monitoring terminal is a small device integrated on a printed-circuit board (PCB) board. The entire system is composed of a microprocessor (CPU) and its peripheral devices [sensor module, data-acquisition (DAQ) module, storage module, communication module, signal preconditioning module, and power supply]. The microprocessor controls the entire system and performs DAQ of the magnetic signal continuously. The information in the signal can be extracted by simple analysis (e.g., amplitude calculation). Once a certain change in the signal is detected, the data are stored and sent to the center station through the communication channel. Since the system aims at serving a mountainous area, a radio station communication solution (i.e., not dependent on commercial service) is preferable. The sensor module is composed of a magnetic sensor chip capable of measurement in the x, y, and z axes and its amplifying and filtering circuits. The sensor is designed to be independent of the disturbance coming from the power supply of the monitoring unit by separating it from the main board. The entire system can be powered by a solar power module which is composed of a solar panel, a charger, and a battery, or alternatively, it can be powered through coupling with the transmission lines.

C. Calculation of the Sensor Output

The magnetic field of current-carrying transmission-line conductors can be calculated by Maxwell's equations. Under certain assumptions, an analytical expression about the relative position between the measured point and the conductors can be

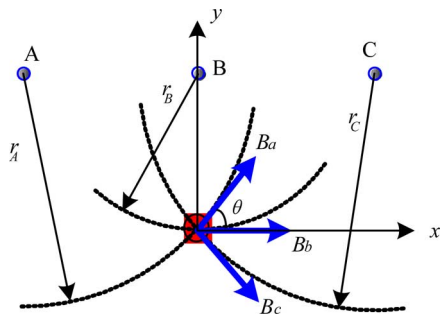

Fig. 3. Calculation of the magnetic field at the point of sensor head. The direction of current is assumed to be along the z axis, which is pointing toward the observer.

formed. Since there are many types of towers and the tower configuration affects the distribution of the magnetic field, the following calculation and simulation are based on a typical 500-kV transmission tower shown in Fig. 2, where the length of the insulator string is assumed to be 4 m, and the sensor is installed at the middle of the tower (18 m above ground level). Fig. 3 shows the decomposition of the resulting magnetic field at the measurement point which can be written as (by assuming that the conductors have no sag and the transmission lines are infinitely long with respect to the distances between the measurement point and the conductors)

$$\begin{aligned}\vec{B} &= \hat{\mathbf{i}}_{\mathbf{x}} B_x + \hat{\mathbf{i}}_y B_y + \hat{\mathbf{i}}_z B_z \\ &= \hat{\mathbf{i}}_{\mathbf{x}}(B_b + (B_a + B_c)\cos\theta) + \hat{\mathbf{i}}_y((B_a - B_c)\sin\theta) + \hat{\mathbf{i}}_z 0\end{aligned} \tag{1}$$

where B_a, B_b, and B_c are the magnetic-field components generated by phase currents i_A, i_B, and i_C, respectively; and $\hat{\mathbf{i}}_{\mathbf{x}}, \hat{\mathbf{i}}_y$, and $\hat{\mathbf{i}}_z$ are the unit vectors along the x, y, and z-axes respectively.

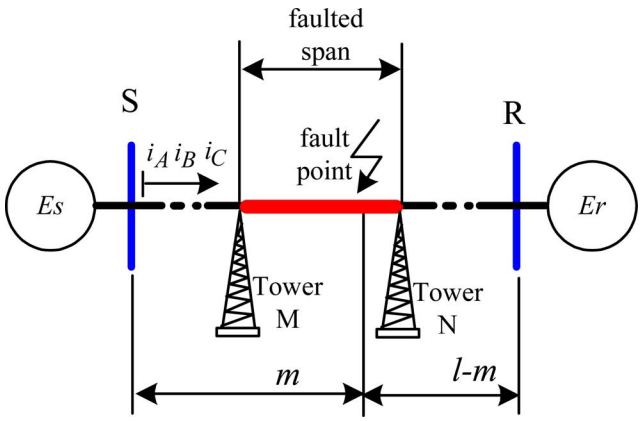

Fig. 4. System diagram of the test system in the numerical simulation (l : the total length of the transmission line; m : distance from the sending end to the fault location).

If the system is not symmetric, the magnetic field should be calculated according to the Biot–Savart law. However, for simple estimation, the effect of conductor sag is neglected (refer to Section V), and the line is assumed to be of infinite length, then B_a, B_b, and B_c can be calculated as

$$B_a = \frac{\mu_0 i_A}{2\pi r_A}, \quad B_b = \frac{\mu_0 i_B}{2\pi r_B}, \quad B_c = \frac{\mu_0 i_C}{2\pi r_C} \tag{2}$$

where μ_0 is the the magnetic constant, and r_A, r_B and r_C are defined in Fig. 3.

D. Location of the Fault

Since the three components of the magnetic field in the 3-D space can be separately measured by MR sensors, they can be used to derive the change in the three-phase current. For a radial transmission system, in which only the sending end has power sources, it is simple to locate the fault point by simply checking where short-circuit current exists in the transmission lines. The output of the terminal closest to the fault point can only be used for qualitative analysis because its output may be affected by the fault (noting that the infinite length assumption may not be true in this case). However, the other outputs can be used to identify the type of faults. For a two-ended system [i.e., both sides have power sources (e.g., tie line)], the fault can be located and analyzed by simply noting that the short-circuit level at the two sides is different. Since the fault span can be accurately located, it is relatively easy to find the exact fault location, even for the nonpermanent fault.

IV. Numerical Simulation

In this section, different cases are studied. All of the case studies are based on the system shown in Fig. 4. The parameters of the system are listed in Table I. Assume that a load of 630 MW is being delivered from the sending end to the receiving end of a power system. In the following numerical simulations, it is assumed that the fault occurs at 0.1 s and disappears at 0.2 s. In all cases, the tower configuration as shown in Fig. 2 is used. With these parameters and assumptions, a distributed model was built and various simulations were performed.

TABLE I
Parameters of the Transmission Line Under Test

Voltage (kV)		*500*	*Line length (km)*		*200*
Sending end short-circuit level (MVA)		54560	Receiving end short-circuit level (MVA)		43300
Positive sequence parameters	R_{pos} (Ω/km)	0.022	Zero sequence parameters	R_{zero} (Ω/km)	0.170
	L_{pos} (mH/km)	0.940		L_{zero} (mH/km)	2.37
	C_{pos} (μF/km)	0.0122		C_{zero} (μF/km)	0.0065

f = 50Hz

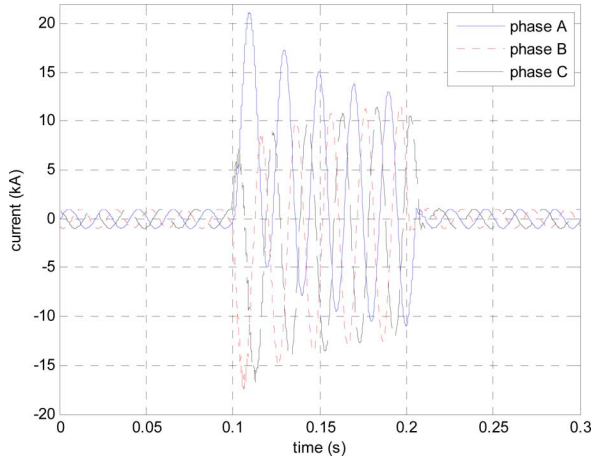

Fig. 5. Typical waveform of the current flowing in three phases during the occurrence of a three-phase short-circuit fault (m = 100 km).

A. Location of Fault Span

Typical faults on transmission lines include single-phase short circuit, double-phase short circuit, and three-phase short circuit. In the impedance-based approach, the effect of the fault resistance and ground resistance must be considered. In the proposed scheme, these effects do not affect the accuracy of the location.

Fig. 5 shows the waveform of the current measured at the tower right ahead of the fault point, under the condition where a three-phase short circuit occurs at the middle of the transmission line. When the three-phase short circuit occurs, the measured magnetic field is increased. The ratio of the magnetic field during the fault to that during the normal situation is the same as the ratio of the short-circuit current to the current at normal condition (as discussed in the previous section), provided that the transient process is not considered. The transient generally further increases the value of the magnetic field.

In order to obtain a full view of the transient process along the entire transmission line to help find the fault point, the magnetic field measured at every tower along the transmission line, which connects two systems, is plotted in Fig. 6. In the figure, the x axis represents the evolution of time (during the lifecycle of a fault, that is, prefault, fault, and postfault), the y axis represents the distribution along the transmission line (0 to the length of the line), and the z axis represents the measured magnetic field. Note that the high magnitude at the beginning of the fault is caused by the decaying dc components in the three-phase currents. The magnitude of the magnetic field at steady state

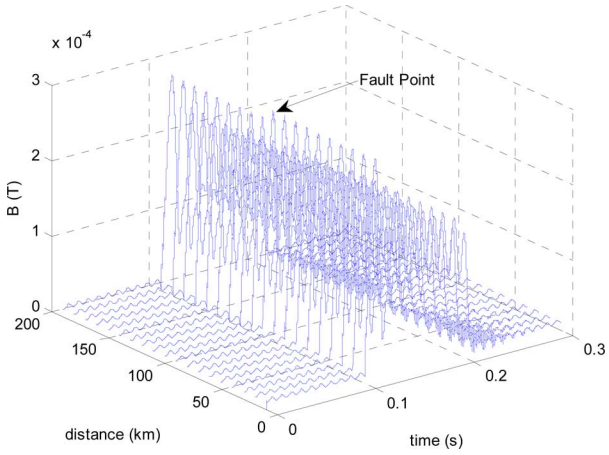

Fig. 6. Distribution of the magnetic field along the transmission line under three-phase short-circuit condition ($m = 100$ km).

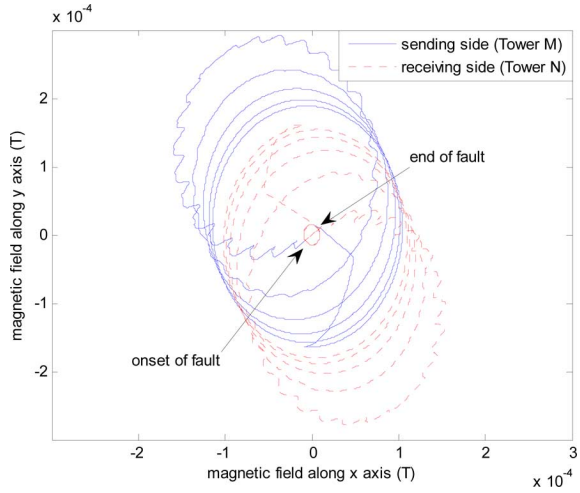

Fig. 7. Direction and magnitude of the magnetic field under the three-phase short-circuit condition (fault occurs at 0.2 s and cleared at 0.3 s, $m = 100$ km).

under fault condition is determined by the short-circuit levels of the two systems connected at two sides. The difference in the short-circuit level can help locate the fault to a span by simply comparing the value of the measured magnetic field. It is noted that at one side, although there is a difference in the measured magnetic field along the transmission line, the difference is very small. This may help a lot considering that the data at certain monitoring terminals may not be collected back in time due to component failure. Due to this reason, any data from the monitoring terminal can be used to identify the fault type, which is discussed in the following section.

If the fault occurs at a point where the short-circuit level at two sides is almost the same, making the magnitude of the magnetic field at two sides very close, then the direction of the magnetic field may be a good indicator of determining the fault span in this case. The magnitude and direction of the magnetic field measured at the two sides (tower M and N in Fig. 4) of the fault point are shown in Fig. 7. In the figure, the small circle at the center describes the magnetic field under normal conditions. Since the radial component (z component in Fig. 3) is generally zero, therefore, only B_x and B_y are plotted. During the life cycle of a fault, B_x and B_y evolve with time. It is shown in the figure that when the system is under normal state, the measured magnetic field at the M and N points have the same direction and magnitude; however, once a fault is initiated, they almost have the opposite direction. If the fault disappears or is cleared by reclosure, the two measured magnetic fields move back to the same point again (the center small circle).

B. Identification of the Fault Type

The measured magnetic field can be used for not only locating the fault but also for identifying the fault type. According to (1) and (2), when a fault occurs, the type of fault can be identified according to the magnitude and direction of the measured magnetic field. Since the short-circuit current is generally much larger than the normal current, the magnetic field caused by current flowing in the unfaulted phase can be neglected.

Therefore, when a single-phase fault occurs, the measured magnetic field satisfies the following conditions (refer to Fig. 3 for the meaning of the parameters):

$$\begin{cases} \dfrac{B_y}{B_x} \approx \dfrac{\sin\theta}{\cos\theta} = tg\theta, & \text{fault at phase A} \\ B_y \approx 0, & \text{fault at phase B} \\ \dfrac{B_y}{B_x} \approx \dfrac{-\sin\theta}{\cos\theta} = -tg\theta, & \text{fault at phase C} \end{cases} . \quad (3)$$

Fig. 8 displays the measured magnetic fields under the single-phase short circuit and Fig. 9 displays the calculated output of the sensor along different directions. It is observed that (3) is true.

When a double-phase fault occurs, one should distinguish the difference between line-to-line fault and double-line-to-ground fault. When the line-to-line fault is considered (transient neglected), the relation among the measured magnetic-field components according to (1) is (refer to Fig. 3 for the meaning of the parameters)

$$\begin{cases} \dfrac{B_y}{B_x} \approx \dfrac{\frac{1}{r_A}\sin\theta}{\frac{1}{r_B}+\frac{1}{r_A}\cos\theta}, & \text{AB line-to-line fault} \\ B_x \approx 0, & \text{AC line-to-line fault} \\ \dfrac{B_y}{B_x} \approx \dfrac{-\frac{1}{r_C}\sin\theta}{\frac{1}{r_B}+\frac{1}{r_C}\cos\theta}, & \text{BCline-to-line fault} \end{cases} . \quad (4)$$

When a double-line-to-ground fault occurs, there is no such simple relation among the components. However, by incorporating the estimation of the short-circuit current (since the fault point is known), the fault type can be identified. Table II lists the characteristics under different fault conditions to facilitate the identification. The identification procedure may consist of the following steps:

Step 1) locating the fault according to the data sent back from the terminal installed along the transmission line;

Step 2) approximately estimating the short-circuit current level with the fault distance determined by Step 1);

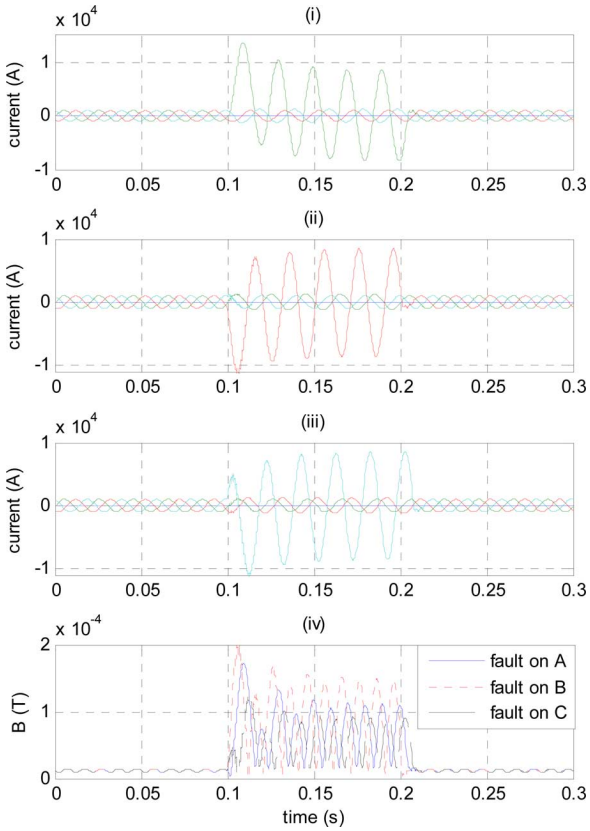

Fig. 8. Magnetic field under the single-phase fault condition. (a) Current waveform under fault on phase A. (b) Current waveform under fault on phase B. (c) Current waveform under fault on phase C. (d) The resulting magnetic-field waveform under the single-phase short-circuit condition.

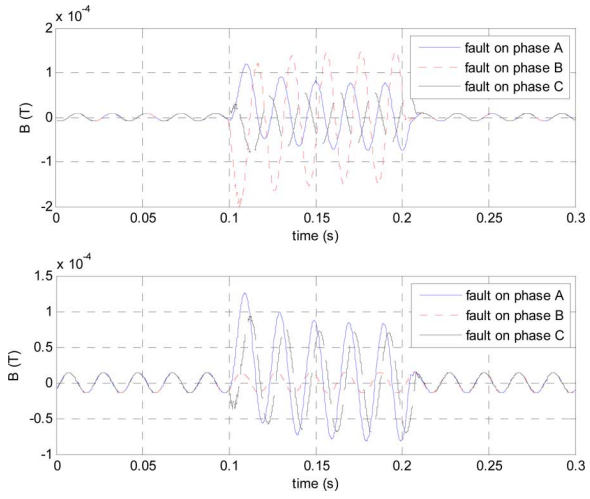

Fig. 9. Measured magnetic fields along different axes under single-phase short-circuit conditions. (The top figure shows the magnetic-field waveform along the x axis while the bottom figure shows the magnetic-field waveform along the y axis; $m = 100$ km.)

Step 3) comparing the measured magnetic field and the calculated value to determine whether the fault belongs to single-phase fault, double-phase fault, or three-phase fault (third column of Table II);

TABLE II
IDENTIFICATION OF THE FAULT TYPE WITH MAGNETIC-FIELD MEASUREMENT

Fault		Characteristics for identification	
		field strength	Supplementary rules
Three phase fault		Largest	All components are the largest
Double line-to-line fault	AB	Medium magnetic field	Satisfies the 1st equation of (4)
	AC		Satisfies the 2nd equation of (4)
	BC		Satisfies the 3rd equation of (4)
Double line-to-ground fault	AB		y component is $1/\sqrt{3}$ of that in three phase fault and $B_y / B_x > 0$
	AC		y component is as large as in three phase fault
	BC		y component is $1/\sqrt{3}$ of that in three phase fault and $B_y / B_x < 0$
Single phase fault	A	Smallest magnetic field	Satisfies the 1st equation of (3)
	B		Satisfies the 2nd equation of (3)
	C		Satisfies the 3rd equation of (3)

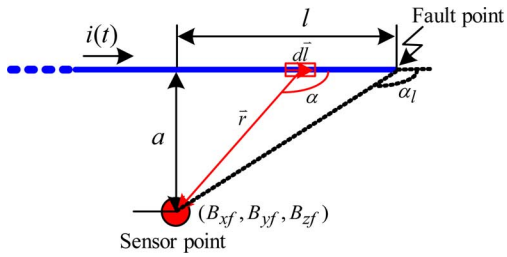

Fig. 10. Estimation of the fault distance in a fault span.

Step 4) further determine the type of the fault according to (3), (4), and the rules in Table II.

Step 5) locating within the fault span according to the result of previous location and identification, which is discussed in the following section.

C. Location Within the Fault Span

The previously described method can locate the fault span. It is observed that the measured magnetic fields have no significant difference along the faulted transmission line. However, the measured magnetic fields at the two sides (e.g., the M and N in Fig. 4) of the fault span are different. This difference can be used to estimate the distance between the fault point and the tower. Fig. 10 shows the model for estimation of the distance to a tower in a faulted span for a single conductor. Assuming that the sensor is installed under a faulted conductor on which a current $i\ (t)$ is flowing through at a distance of a. If a is far less than the length of a span, according to Biot-Savart law, the ratio of the measured magnetic field beside the fault point to the other measured magnetic field is

$$\frac{B_{xf}}{B_x} = \frac{B_{yf}}{B_y} = \frac{1 - \cos\alpha_f}{2} \tag{5}$$

where B_x and B_y are assumed to be the measured magnetic-field components far away from the fault span.

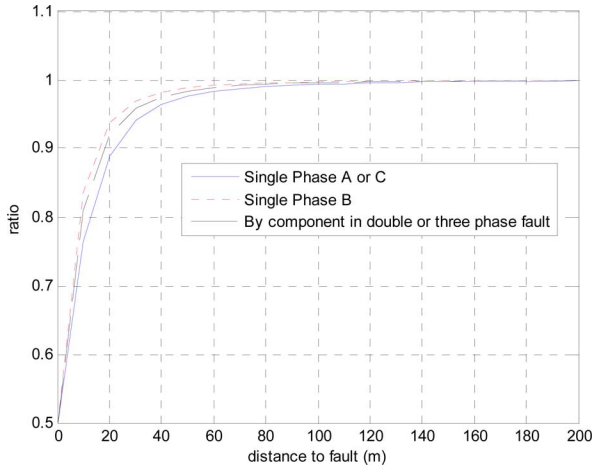

Fig. 11. Ratio of the magnetic field measured at the tower next to the fault point to that measured at the other towers under different fault types.

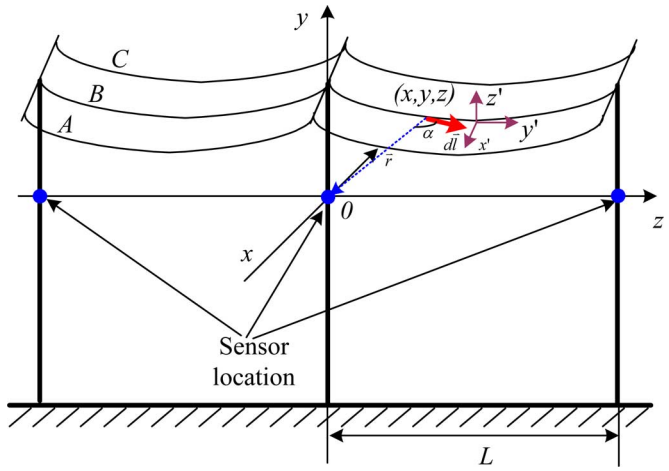

Fig. 12. Magnetic field generated by the transmission system considering sag effect.

For double-phase and three-phase faults, it is more complex because a simple analytical expression cannot be found due to the difference in phase angle in the three phases. However, once the type of the fault is determined, the location within the fault span can be accomplished using the B_x or B_y component. For example, in single-phase fault cases, the location can be estimated using either B_x or B_y; under double-phase and three-phase line-to-line fault, one can choose the B_y component to compare. Fig. 11 shows the ratio of the magnetic field measured at the tower next to the fault point to that measured at other towers as a function of the fault location. When the fault distance is less than 100 m, a significant difference can be observed. If no difference is observed, it can be concluded that the fault point is out of the range of 100 m, which can also help the maintenance crew expedite the location procedure.

V. Error Estimation and Discussion

The error of this proposed scheme comes from the following aspects: 1) the measurement error of the device, which is highly dependent on the characteristics of the magnetoresistive sensor and the signal conditioning circuit; 2) the error caused by the sag of the transmission lines; and 3) when the approach is used for multiple conductor transmission systems (e.g., the typically used quad-bundled conductor), the nonuniform distribution of the current will cause a certain amount of error, or if twisting of conductors occurs, it may bring errors to the measurement of the magnetic field. Other factors, such as the skin effect, can be neglected since the sensor is placed far enough away from the conductors.

A. Measurement Error

One of the advantages of the magnetoresistive sensor is that the solid-state sensors have typical bandwidths in the megahertz range and resolutions of tens of microgauss [19]. And modern circuit design technology can easily facilitate a signal conditioning circuit of megahertz bandwidth. However, if only for fault-location purposes, it is reasonable to limit the sampling frequency to less than 2000 Hz. In the lab experiment, a test 12-b analog-to-digital converter can easily limit the measurement error in a range of 1%.

B. Sag Effect

When sag of the conductors is considered, the magnetic field at the measurement point will be different from that generated by the current-carrying power-line conductors, which are assumed to be straight horizontal wires. The evaluation of the error caused by sag can be accomplished with the combination of Biot–Savart law and catenary equation [20]. For the evaluation, assume that the sags of two adjacent leveled spans are symmetric and all three-phase conductors have the same amount of sag (different sag can be similarly handled, referring to the Appendix), as shown in Fig. 12. To simplify the calculation, two coordinate systems (x, y, z) and (x', y', z') are used. The (x, y, z) coordinate system is centered at the location of the sensor, in order to be congruent with the coordinate system in Fig. 3, while (x', y', z') is centered at the maximum sag point of the middle phase conductor (phase B in Fig. 12), in order to be congruent with the popular use of the catenary equation.

Considering phase conductor B in Fig. 12, the governing catenary equation in the (x', y', z') coordinate system is

$$z' = \frac{1}{\alpha}(\cosh(\alpha y') - 1), \quad -\frac{L}{2} \le y' \le \frac{L}{2} \tag{6}$$

where L is the length of the span, and α is a constant determined by the mechanical parameters of the transmission lines.

With the symmetry assumption, the magnetic field generated by phase A, B, and C at the middle sensor in Fig. 12 can be obtained by the following equations (refer to the Appendix of the paper for more detailed information):

$$\vec{B}_a = \frac{\mu_0 i_A}{2\pi} \int_{-L/2}^{L/2} \left[\begin{array}{c} \frac{z_0' - \frac{1}{\alpha}(\cosh\alpha y' - 1) + (y' - y_0')\sinh\alpha y'}{M_a} \hat{\mathbf{i}}_{x'} \\ + \frac{(x_0' - k)\sinh\alpha y'}{M_a} \hat{\mathbf{i}}_{y'} + 0\hat{\mathbf{i}}_{z'} \end{array} \right] dy' \tag{7}$$

$$\vec{B}_b = \frac{\mu_0 i_B}{2\pi} \int_{-L/2}^{L/2} \left[\begin{array}{c} \frac{z_0' - \frac{1}{\alpha}(\cosh\alpha y' - 1) + (y' - y_0')\sinh\alpha y'}{M_b} \hat{\mathbf{i}}_{x'} \\ + \frac{x_0'\sinh\alpha y'}{M_b} \hat{\mathbf{i}}_{y'} + 0\hat{\mathbf{i}}_{z'} \end{array} \right] dy' \tag{8}$$

TABLE III
EVALUATION OF THE SAG EFFECT ON THE CALCULATION OF THE MAGNETIC FIELD

Phase conductors	Coefficient along three spatial axes					
	Straight horizontal wire			Sag effect considered		
	x	y	z	x	y	z
A	0.0423	0.0453	0	0.0434	0.0469	0
B	0.0909	0	0	0.0954	0	0
C	0.0423	0.0453	0	0.0434	0.0469	0

(Span: 400m; Phase Space: 11.8m; Sag: 5m)

$$\vec{B}_c = \frac{\mu_0 i_C}{2\pi} \int_{-L/2}^{L/2} \left[\begin{array}{l} \frac{z_0' - \frac{1}{\alpha}(\cosh \alpha y' - 1) + (y' - y_0') \sinh \alpha y'}{M_c} \hat{\mathbf{i}}_{x'} \\ + \frac{(x_0' + k) \sinh \alpha y'}{M_c} \hat{\mathbf{i}}_{y'} + 0 \hat{\mathbf{i}}_{z'} \end{array} \right] dy' \tag{9}$$

where $\hat{\mathbf{i}}_{x'}, \hat{\mathbf{i}}_{y'}$ and $\hat{\mathbf{i}}_{z'}$ are the unit vectors along the x', y', and z' axes, respectively; (x_0', y_0', z_0') is the coordinate of the sensor point under the (x', y', z') coordinate system (origin in the (x, y, z) coordinate system), and k is the space between the phase conductor (11.8 m as shown in Fig. 2)

$$M_a = \left[(x_0' - k)^2 + (y_0' - y')^2 + (z_0' - \frac{1}{\alpha}(\cosh \alpha y' - 1)^2 \right]^{\frac{3}{2}} \tag{10}$$

$$M_b = \left[x_0'^2 + (y_0' - y')^2 + \left(z_0' - \frac{1}{\alpha}(\cosh \alpha y' - 1) \right)^2 \right]^{\frac{3}{2}} \tag{11}$$

$$M_c = \left[(x_0' + k)^2 + (y_0' - y')^2 + (z_0' - \frac{1}{\alpha}(\cosh \alpha y' - 1)^2 \right]^{\frac{3}{2}}. \tag{12}$$

Comparing these equations with (2), it is clear that one only needs to compare the definite integrals with $(1)/(r_A), (1)/(r_B)$ and $(1)/(r_C)$ in (2) and their components along the three spatial axes, respectively. For a transmission system configured as shown in Fig. 2, and assuming the span length L at 400 m, further assuming a sag of 5 m on all three-phase conductors, the comparison is shown in Table III. It is shown that the error is always less than 5%.

C. Error of Bundled Conductors

To evaluate the error caused by bundled conductors, a typical "quad-bundle" configuration with 0.3-m spacing is considered. For example, if phase B is considered, and further assuming the current is uniformly flowing in four conductors, (13), shown at the bottom of the page, can be used to evaluate the error by assuming that the magnetic field is generated by a single conductor. Numerical results show that for the configuration discussed in this paper, this may only cause 0.01% error.

TABLE IV
COMPARISON OF AVAILABLE FAULT-LOCATION APPROACHES

Approaches	*Descriptions*	
Impedance measurement based approach	Requirements	■ Measurement of voltage and current ■ Parameters to know: Line length and transmission impedance
	Advantages	■ No additional hardware cost
	Disadvantages	■ Have to assume homogeneity in line parameter ■ Relative location error ■ Not work well for fault with fault resistance ■ Performance is highly dependent on signal processing techniques ■ Affected by CT saturation ■ Not work for open-circuit fault ■ Hard to map the electrical distance to actual geographical location
Traveling wave based approach	Requirements	■ Measurement of current or voltage traveling wave ■ Parameters to know: Line length and wave speed
	Advantages	■ Work for open-circuit fault
	Disadvantages	■ Has to assume uniform wave speed ■ High-speed data acquisition, high cost ■ Relative location error ■ Performance is highly dependent on signal processing techniques ■ Hard to map the electrical distance to actual geographical location
Magnetic field measurement based	Requirements	■ Measurement of current ■ Parameters to know: none
	Advantages	■ Non-contact ■ Absolute location error: one span ■ Independent of distributed line parameter ■ Not affected by saturation ■ Location of fault is mapped to actual geographical location and can be easily visualized
	Disadvantages	■ Distributed measurement, requiring reliable data communication ■ Not work for open-circuit fault

D. Discussion

According to error estimate, one can safely conclude that the error brought by the sag and bundled conductor will not affect the effectiveness of the approaches discussed in this paper; hence, the proposed approach is feasible. Table IV summarized the general requirements, advantages, and disadvantages of the available approaches for the fault location of the power transmission line. One of the great advantages of the proposed approach is that its maximum location error is one span, and it does not assume a homogeneous line while traditional approaches have to rely on the assumption of the homogeneous line, and the evaluation of the performance is obtained by the fault-location error defined in IEEE PC37.114 [6], that is, a percentage error in the fault-location estimate based on the total line length

$$\text{error} = \frac{\text{instrument reading-exact distance to the fault}}{\text{total line length.}} \tag{14}$$

$$\left(\frac{1}{2} \left(\frac{1}{\sqrt{(r_B - 0.15)^2 + 0.15^2}} + \frac{1}{\sqrt{(r_B + 0.15)^2 + 0.15^2}} \right) - \frac{1}{r_B} \right) / \left(\frac{1}{r_B} \right). \tag{13}$$

This means that even a small error may cause a large physical distance for a long transmission line. Furthermore, unlike the impedance-measurement-based approach, the ground resistance does not affect the performance of the proposed approach.

The only disadvantages of the proposed approach are that it has to rely on distributed measurement and, due to the reason that it depends on current measurement, it cannot be used for open-circuit fault detection. However, considering the fact that the most common and dangerous fault that occurs in a power system is the short circuit, not working for an open-circuit fault would not limit the use of the proposed approach. And with modern communication, information, and integrated-circuit technology, it is very easy to implement such a distributed measurement system.

VI. Conclusion and Future Works

As the MEMS packaging technology and magnetoresistance material technology are progressing rapidly, MR sensors based on the magnetoresistance effect, which can carry out the point measurement of the magnetic field, may bring revolutionary change for measurement techniques in power systems. In this paper, a novel approach based on the noncontact measurement of magnetic field is proposed for the fault location of overhead transmission lines. By checking whether the short-circuit current exists in the transmission line at the position of an installed monitoring terminal, the fault span can be located which may greatly reduce the uncertainty in searching for fault location and, hence, improve the efficiency. Moreover, the solution is low cost and more effective for finding the exact fault location even for nonpermanent faults. After the fault span is located, the measured magnetic field can be used to further identify the fault type and locate within the fault span. The numerical simulations and error estimate in this paper verify the proposed scheme.

In future work, other types of tower configurations or their combinations should be considered to extend the applications. Moreover, the configuration of the sensor array needs to be further modified and improved in order to extend the application into the fault location for double or multicircuit transmission lines.

Appendix

For a transmission system as shown in Fig. 12, the calculation of the magnetic field at an arbitrary point in the space can be implemented as follows. Consider a small section of any one of the transmission lines $d\vec{l}$. According to the Biot–Savart law, it generates a magnetic field at a point (x_0', y_0', z_0'),

$$d\vec{B} = \frac{\mu_0 I}{4\pi}\frac{d\vec{l}\times\vec{r}}{|\vec{r}|^3}. \tag{A1}$$

According to (6), $d\vec{l}$ can be expressed as

$$\begin{aligned} d\vec{l} &= dy\hat{\mathbf{i}}_y' + dz'\hat{\mathbf{i}}_z' \\ &= 0\hat{\mathbf{i}}_x' + dy\hat{\mathbf{i}}_y' + \frac{dz'}{dy'}dy'\hat{\mathbf{i}}_z'. \end{aligned} \tag{A2}$$

With $(dz')/(dy') = \sinh\alpha y'$. And

$$\vec{r} = (x_0' - x')\hat{\mathbf{i}}_x' + (y_0' - y')\hat{\mathbf{i}}_y' + \left(z_0' - \frac{1}{\alpha}(\cosh\alpha y' - 1)\right)\hat{\mathbf{i}}_z' \tag{A3}$$

Substitute (A2) and (A3) into (A1), and if only one span is considered, the magnetic field generated at point (x_0', y_0', z_0') would be

$$\vec{B} = \frac{\mu_0 i}{4\pi}\int_{-L/2}^{L/2}\left[\begin{array}{l}\frac{z_0' - \frac{1}{\alpha}(\cosh\alpha y' - 1) + (y' - y_0')\sinh\alpha y'}{|\vec{r}|^3}\hat{\mathbf{i}}_{x'} \\ +\frac{(x_0' - x')\sinh\alpha y'}{|\vec{r}|^3}\hat{\mathbf{i}}_{y'} + \frac{-(x_0' - x')}{|\vec{r}|^3}\hat{\mathbf{i}}_{z'}\end{array}\right]dy'. \tag{A4}$$

When only one of the three conductors is considered (the other two phase currents are assumed to be zero) and since the two adjacent spans are symmetric, integration in two spans[1] will double the magnetic field along $\hat{\mathbf{i}}_x'$ and $\hat{\mathbf{i}}_z'$ directions, and cancel the magnetic field along the $\hat{\mathbf{i}}_y'$ direction. When the three-phase conductors are considered separately, (8)–(12) can be obtained.

References

[1] T. Adu, "A new transmission line fault locating system," *IEEE Trans. Power Del.*, vol. 16, no. 4, pp. 498–1503, Oct. 2001.

[2] H. X. Ha, B. H. Zhang, and Z. L. Lv, "A novel principle of single-ended fault location technique for EHV transmission lines," *IEEE Trans. Power Del.*, vol. 18, no. 4, pp. 1147–1151, Oct. 2003.

[3] Y. Liao and M. Kezunovic, "Optimal estimate of transmission line fault location considering measurement errors," *IEEE Trans. Power Del.*, vol. 22, no. 3, pp. 1335–1341, Jul. 2007.

[4] T. Bouthiba, "Fault location in EHV transmission lines using artificial neural networks," *Int. J. Appl. Math. Comput. Sci.*, vol. 14, no. 1, pp. 69–78, 2004.

[5] M. Bockarjova, A. Sauhats, and G. Andersson, "Statistical algorithms for fault location on power transmission lines," *Proc. IEEE Russia Power Tech.*, pp. 1–7, 2005.

[6] *IEEE Guide for Determining Fault Location on AC Transmission and Distribution Lines*, IEEE Std C37.114-2004, 2005, Power Syst. Relay. Comm., E-ISBN: 0-7381-4654-4.

[7] A. Abur and F. H. Magnago, "Use of time delays between modal components in wavelet based fault location," *Int. J. Elect. Power Energy Syst.*, vol. 22, no. 6, pp. 397–403, 2000.

[8] S. M. Brahma, "Iterative fault location scheme for a transmission line using synchronized phasor measurements," *Int. J. Emerging Elect. Power Syst.*, vol. 8, no. 6, pp. 1–14, 2007, Article 2.

[9] C. S. Yu, C. W. Liu, S. L. Yu, and J. A. Jiang, "A new PMU-based fault location algorithm for series compensated lines," *IEEE Trans. Power Del.*, vol. 17, no. 1, pp. 33–46, Jan. 2002.

[10] *Electrical Transmission and Distribution Reference Books*. Jefferson City, MO: ABB Power T&D Co., 1997, pp. 32–63.

[11] A. Sauhats and M. Danilova, "Fault location algorithms for super high voltage power transmission lines," in *Proc. IEEE Power Tech Conf.*, 2003, pp. 1–6.

[12] R. K. Rajput, *Power System Engineering*. New Delhi, India: Laxmi Publication, 2006, p. 769.

[13] A. Edelstein, "Advances in magnetometry," *J. Phys.: Condensed Matter*, no. 19, pp. 1–28, 2007.

[14] M. Vopalensky, A. Platil, and P. Kaspar, "Wattmeter with AMR sensor," *Sens. Actuators A, Phys.*, pp. 303–307, 2005, 123-124.

[15] C. Reig, M. D. Cubells-Beltran, and D. R. Munoz, "Magnetic field sensors based on giant magnetoresistance (GMR) technology: Applications in electrical current sensing," *Sens.*, no. 9, pp. 7919–7942, 2009.

[16] J. W. Stahlhut, G. T. Heydt, and E. Kyriakides, "Innovative sensory concepts for power systems," in *Proc. 38th Annu. North Amer. Power Symp.*, IL, 2006, pp. 397–404.

[1]It is not necessary to integrate more than two spans, because of the fast decaying of the magnetic field as the distance increases, due to the term $1/|\vec{r}|^3$ in (A4).

[17] Z. Zhang and L. Di Rienzo, "Optimization of magnetic sensor arrays for current measurement based on swarm intelligence and D-optimality," *Int. J. Comput. Math. Elect. Electron. Eng.*, vol. 28, no. 5, pp. 1179–1190, 2009.
[18] G. D. Antona, L. D. Rienzo, R. Ottoboni, and A. Manara, "Processing magnetic sensor array data for AC current measurement in multiconductor systems," *IEEE Trans. Instrum. Meas.* , vol. 50, no. 5, pp. 1289–1295, Oct. 2001.
[19] B. Wincheski and J. Simpson, "Development and application of wide bandwidth magneto-resistive sensor based eddy current probe. Review of progress in quantitative nondestructive evaluation," in *Proc. AIP Conf.*, 2011, vol. 30, pp. 388–395.
[20] A. V. Mamishev, R. D. Nevels, and B. D. Russell, "Effects of conductor sag on spatial distribution of power line magnetic field," *IEEE Trans. Power Del.*, vol. 11, no. 3, pp. 1571–1576, Jul. 1996.

Qi Huang (S'99–M'03–SM'09) was born in Guizhou Province, China. He received the B.S. degree in electrical engineering from Fuzhou University, Fuzhou, China, in 1996, the M.S. degree from Tsinghua University, Beijing, China, in 1999, and the Ph.D. degree from Arizona State University, Tempe, in 2003.

Currently, he is a Professor at the Sichuan Provincial Key Lab of Power System Wide-Area Measurement and Control, University of Electronic Science and Technology of China (UESTC), Chengdu, and the Deputy Dean of School of Energy Science and Engineering, UESTC, and the Director of Sichuan State Provincial Lab of Power System Wide-Area Measurement and Control. His current research and academic interests include power system high-performance computing, power system instrumentation, power system monitoring and control, as well as the integration of distributed generation into the existing power system infrastructure.

Wei Zhen was born in 1957 in Hebei Province, China. He received the B.S. degree in power system automation from Xi'an Jiaotong University (XJTU), Xi'an, China, in 1982.

After that, he was a Senior Engineer with the Sichuan Provincial Key Lab of Power System Wide-Area Measurement and Control, and Sichuan Electric Power Test and Research Institute, Chengdu, and Director of the Power System Engineering Research Center. His research fields include power system relay protection, power system analysis, and state-of-the-art technology development.

Philip W. T. Pong received the Ph.D. degree in engineering from the University of Cambridge, Cambridge, U.K., in 2005.

Currently, he is a Physicist and Electrical Engineer, working on magnetoresistive magnetic-field sensors and smart grid in the Department of Electrical and Electronic Engineering (EEE), the University of Hong Kong (HKU), Hong Kong, China. After working as a Postdoctoral Researcher in the Magnetic Materials Group, National Institute of Standards and Technology (NIST), for three years, he joined the HKU engineering faculty where he is now an Assistant Professor working on tunneling magnetoresistance sensors, and the application of magnetoresistive sensors in smart grid.